SLAC-PUB-2118
May 1978
(T/E)

JETS IN e^+e^- ANNIHILATION*

Gail G. Hanson
Stanford Linear Accelerator Center
Stanford University, Stanford, California 94305, U.S.A.

Abstract: The latest results on R, the ratio of the total cross section for production of multihadronic events to the muon pair production cross section, and inclusive distributions of hadrons from e^+e^- annihilation in the center-of-mass energy range from 2.6 to 7.8 GeV are presented. The evidence for jet structure is reviewed. Inclusive distributions of hadrons in Feynman x, rapidity, and transverse momentum relative to the jet direction are studied. Particular emphasis is placed on the method used to measure these inclusive distributions and the biases which might result from this method.

Résumé: Les résultats les plus récents concernant la mesure de R, rapport de la section efficace totale de production de hadrons à la section efficace de production de paires de muons, ainsi que la mesure des distributions inclusives des hadrons dans les annihilations e^+e^- sont presentés pour des energies dans le centre de masse comprises entre 2.6 et 7.8 GeV. L'evidence d'une structure en jet est passée en revue. Les distributions inclusives des hadrons sont étudiées en fonction de la variable de Feynman x, de la rapidité et du moment transverse par rapport à la direction du jet. L'accent est mis sur la méthode utilisée pour mesurer ces distributions inclusives et sur les biais qui peuvent en résulter.

Talk given at the 13th Rencontre de Moriond on High Energy Leptonic Interactions and High Energy Hadronic Interactions, Les Arcs, Savoie, France, March 12-24, 1978

*Work supported by the Department of Energy.

I. INTRODUCTION

Electron-positron annihilation has proved to be a very fruitful source of exciting new physics. The increase in the total cross section for hadron production was the first hint that a new quantum number - charm - existed.[1] The ψ and ψ' and their associated states were discovered.[2] A heavy lepton τ was found.[3] And finally charmed mesons themselves were isolated and found to be produced copiously in pairs at the ψ''.[4,5]

The reason that e^+e^- collisions are so useful is that the electron and positron predominantly annihilate to form a single virtual photon which subsequently produces a particle-antiparticle pair (e.g., $\tau^+\tau^-$) or a quark-antiquark pair which converts into hadrons. These general theoretical ideas have so far been substantiated by experimental data. One of the predictions of quark-parton constituent models is that at sufficiently high energy multihadronic events produced by e^+e^- annihilation should form two back-to-back jets due to the limiting of transverse momentum relative to the original quark direction.[6] Evidence for such jet structure is seen in e^+e^- annihilation data for center-of-mass energies ($E_{c.m.}$) of 4.8 GeV and greater.[7] If it is true that the jet structure is due to quark jets, then it is of interest to study the inclusive distributions of hadrons relative to the jet direction in order to obtain information about the fragmentation of quarks into hadrons. In this talk I will present hadron inclusive distributions in Feynman x, rapidity, and transverse momentum relative to the jet direction in multihadronic events from e^+e^- annihilation in the $E_{c.m.}$ range from 3.0 to 7.8 GeV.

II. DETECTOR AND EVENT SELECTION

The data for this analysis were taken by the SLAC/LBL magnetic detector collaboration[8] at SPEAR. The SPEAR Mark I magnetic detector is shown schematically in Fig. 1. The detector consisted of a 3-meter long, 3-meter diameter solenoid magnet with a 4 kG magnetic field parallel to the beam direction and wire spark chambers and scintillation counters for triggering and measuring events. The detector axis was centered on the beam direction at one of two interaction regions at SPEAR. Particles entering the detector from the interaction region could pass through, in order: a 150 μm steel vacuum chamber, inner cylindrical scintillation counters used in the trigger to reduce background from cosmic rays, inner multiwire proportional chambers, a system of 4 sets of cylindrical wire spark chambers, an array of trigger time-of-flight scintillation counters, the magnet coil, an array of lead-scintillator shower counters, the iron return yoke of the magnet, and finally wire spark chambers used for muon-hadron separation. The detector extended over 65% of 4π sr solid angle with full acceptance in azimuthal angle and acceptance in polar angle from 50° to 130°. The apparatus was triggered by two or more charged particles which produced

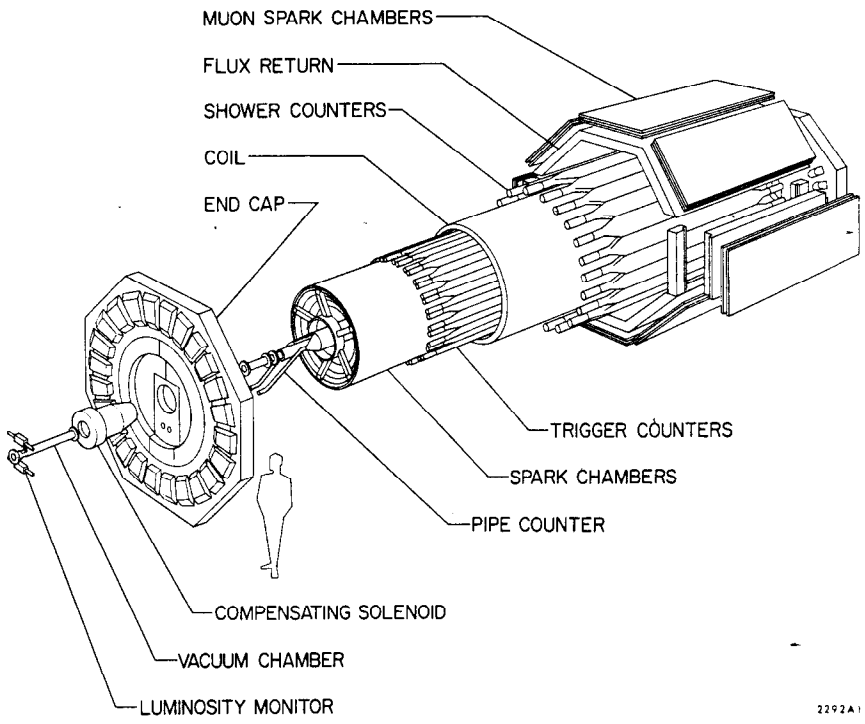

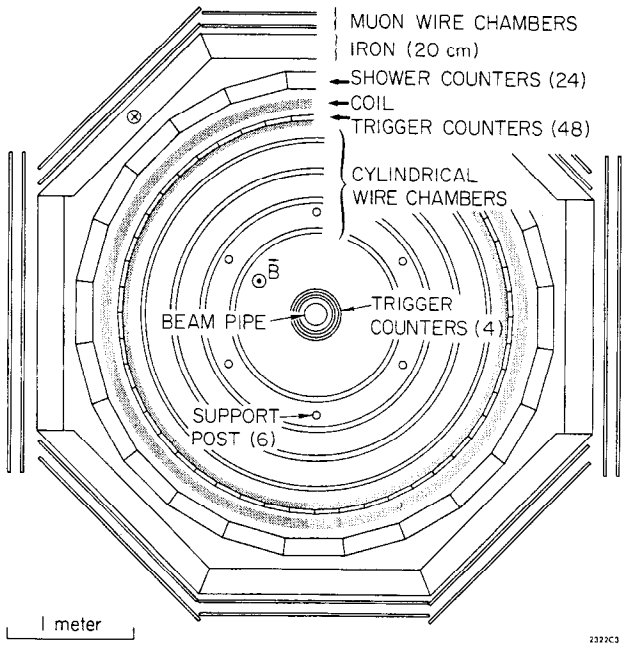

Fig. 1. Schematic diagrams of the SLAC/LBL magnetic detector.

signals in the inner scintillation counters and in at least two outer trigger counters and their associated shower counters. This trigger requirement could be satisfied only by events with two or more charged particles within the detector acceptance and having momenta greater than 200 MeV/c and is mainly responsible for the uncertainties in efficiency calculations.

Events from the QED reactions

$$e^+e^- \rightarrow e^+e^- \text{ (Bhabha scattering)} \tag{1}$$

and

$$e^+e^- \rightarrow \mu^+\mu^- \tag{2}$$

were recorded simultaneously with the multihadronic events and provided a convenient normalization. Of those events originating from the interaction-region fiducial volume, those with two oppositely-charged prongs collinear within 10° were candidates for the QED reactions. Those events in which there were two prongs acoplanar with the incident beam direction by at least 20° and in which both prongs had momenta greater than 300 MeV/c and those with three or more prongs were classified as hadronic. Additional cuts were applied to remove non-collinear two-prong and multiprong events originating from QED processes.

III. TOTAL CROSS SECTION AND INCLUSIVE MOMENTUM DISTRIBUTIONS

The total hadronic cross section was calculated from the total number of multihadronic events detected at each energy $E_{c.m.}$ from 2.6 to 7.8 GeV, corrected for losses due to geometric acceptance, triggering efficiency, cuts, and contamination from other sources. The cross section was normalized to the integrated luminosity obtained from Bhabha scattering events observed in the magnetic detector. Losses due to geometric acceptance, triggering efficiency, and data analysis cuts were estimated using a Monte Carlo simulation, described in more detail in Section IV, in which hadronic events were produced according to a jet model. The Monte Carlo calculation resulted in a matrix of efficiencies for detecting a particular number of charged particles for each charged particle multiplicity in the produced state. Radiative corrections were applied separately for each produced multiplicity. At each energy a produced multiplicity distribution was obtained as the maximum-likelihood solution to an overdetermined set of linear equations. The average detection efficiency, given by the number of detected events divided by the number of produced events, increased monotonically from about 33% at the lowest energy to about 65% at the highest energy. The data were corrected for background from beam-gas scattering (<8% for $E_{c.m.}$ less than 5 GeV and <5% for $E_{c.m.}$ above 5 GeV) and from two-photon processes (<2%) and for losses due to vertex reconstruction outside the interaction-region fiducial volume (5%).

The ratio R of the total hadronic cross section to the theoretical total cross section for production of muon pairs is presented in Fig. 2. Heavy lepton

production, which contributes primarily to the two-prong cross section, has not been subtracted. The errors shown are statistical only. The overall normalization uncertainty is ±10% and a further smooth variation as large as 10% from the lowest energy to the highest energy could arise from systematic errors in the estimation of the detection efficiency. The ψ and ψ' peaks are not shown and the binning of the data between 3.9 and 4.5 GeV is not optimized to show the structure in this region. R is approximately constant at about 2.6 for $E_{c.m.}$ less than 3.5 GeV. Above 4.8 GeV R is again approximately constant at a value of about 5.3. Although the data have been reanalyzed using more sophisticated techniques and more data have been taken, the results for R are very similar to those presented at the 1975 Lepton and Photon Symposium.[9] The values for R presented here are in good agreement with those presented by the DASP collaboration at DORIS, except for the detailed structure in the 4 GeV region, for the energy range between 3.6 and 5.2 GeV which they have measured.[10] The R values from the Pluto collaboration are somewhat lower but are probably consistent within the systematic errors of the two experiments.[11] The mean charged particle multiplicity $\langle n_{ch} \rangle$, obtained as part of the procedure for determining the total cross section, plotted versus the logarithm of $E_{c.m.}$ is presented in Fig. 3. $\langle n_{ch} \rangle$ rises from about 3.5 at the lowest energies to about 5 at

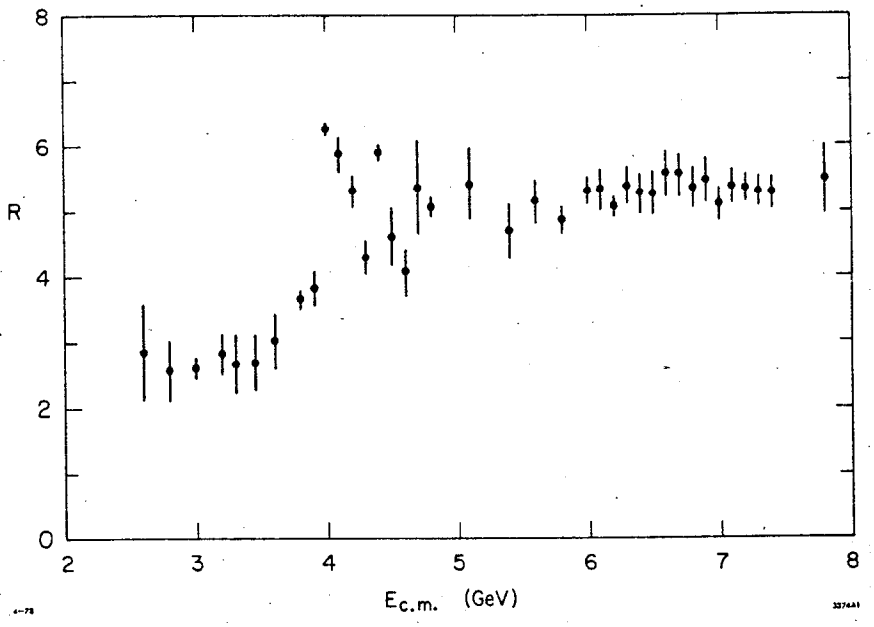

Fig. 2. R vs. $E_{c.m.}$ (heavy lepton production not subtracted).

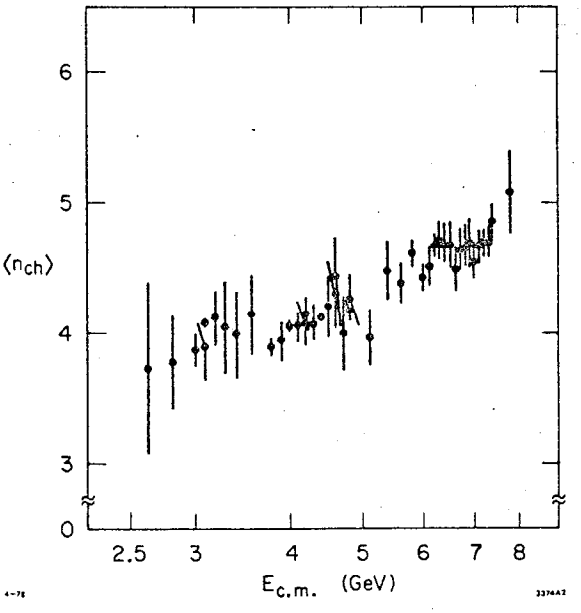

Fig. 3. Mean charged particle multiplicity $\langle n_{ch} \rangle$ vs. $E_{c.m.}$ (heavy lepton production not subtracted).

the highest energies. Heavy lepton production has not been subtracted.

Single particle inclusive momentum distributions have been measured at $E_{c.m.}$ values of 3.0 and 4.8 GeV and in three energy ranges from 5.6 to 7.8 GeV. The momentum distributions are presented in terms of the "experimental" scaling variable x, where

$$x = 2p/E_{c.m.}, \tag{3}$$

and p is the particle momentum. The momentum is used instead of the energy because π's, K's, and p's can be separated unambiguously by our time-of-flight system only for momenta less than 1.1 GeV/c. Only multihadronic events with three or more detected charged particles were used in this analysis and for the analyses in the remainder of this presentation. The two-prong events were not used because they are more subject to background contamination due to beam-gas and two-photon interactions. Because the two-prong events were not used, the inclusive distributions presented here contain little contribution from heavy lepton production.

The detected single particle momentum distributions were corrected for trigger bias, geometric acceptance, and data analysis cuts using the jet model Monte Carlo simulation. The distributions were corrected so as to include multihadronic events with all produced multiplicities, including events with two charged particles. In addition, the Monte Carlo efficiencies contain a momentum-dependent correction for initial-state radiation so that the distributions are radiatively corrected. The effects of this radiative correction are an overall decrease in efficiency because nonradiative events have higher multiplicities than those in which there was significant radiation and an additional decrease in efficiency for large x because events with significant radiation cannot have particles with large x.

The single particle inclusive x distributions are presented in Fig. 4. The quantity plotted is $s\,d\sigma/dx$ ($s = E_{c.m.}^2$) which is expected to scale at very high energies. The area under each curve is equal to $s\,\sigma_T\langle n_{ch}\rangle \propto R\langle n_{ch}\rangle$ (σ_T is the total hadronic cross section), so the area under the curve must increase as the energy increases, even for constant R, since $\langle n_{ch}\rangle$ increases. We see that most of this increase occurs for $x<0.3$. $s\,d\sigma/dx$ roughly scales for $x\geq 0.3$ for the entire energy range. The 3.0 GeV data seem to be systematically high for $x\geq 0.6$; however, systematic errors due to the Monte Carlo corrections at the highest and lowest values of x could be as large as 20%. In addition, the detected two-prong events, which we do not use but correct for, form the largest fraction of the total number of events (25%) at 3.0 GeV. The data for $E_{c.m.} \geq 4.8$ GeV scale rather well for $x \geq 0.2$, although there is a spread of about 20 % from the lowest energy to the highest energies for x between 0.3 and 0.5. More will be said about scaling in Section V when inclusive distributions in Feynman x are discussed.

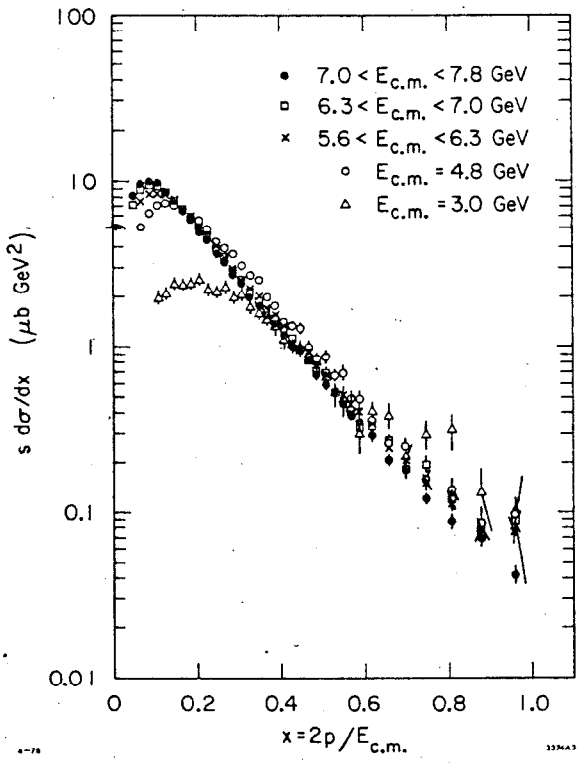

Fig. 4. Single particle inclusive x distributions s dσ/dx vs. x for various $E_{c.m.}$.

Our measurements of s dσ/dx are consistently higher for all x than are those presented by the DASP and PLUTO collaborations.[12] The reason for this difference is not understood. However, the areas under our s dσ/dx curves agree with the independently calculated $\langle n_{ch} \rangle$ from the total cross section determinations.

IV. JET STRUCTURE AND DESCRIPTION OF MONTE CARLO SIMULATION

In quark-parton constituent models for hadron production by e^+e^- annihilation, the e^+ and e^- annihilate to form a virtual photon which subsequently produces a quark-parton pair, each of which decays into hadrons, as shown in Fig. 5. At sufficiently high energy a two-jet structure is expected to arise due to the limited transverse momentum of the hadrons with respect to the original parton direction.[6] The spins of the constituents can, in principle, be determined from the angular distribution of the jets. A review of the jet structure observed in e^+e^- annihilation will be presented in this section.

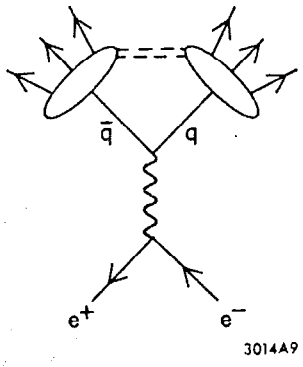

Fig. 5. Quark-parton model picture of production of hadrons in e^+e^- annihilation..

In order to search for jet structure, we find the direction which minimizes the sum of squares of transverse momenta for each event. This direction will be referred to as the observed jet axis. To determine how jet-like an event is, we calculate a quantity which we call the sphericity S:

$$S = \frac{3\left(\sum_i p_{\perp i}^2\right)_{min}}{2\sum_i \vec{p}_i^{\,2}} , \qquad (4)$$

where the numerator is the minimum sum of squares of transverse momenta found in the determination of the observed jet axis. S approaches 0 for events with limited transverse momentum (jet-like events) and approaches 1 for events with large multiplicity and isotropic particle distributions.

Since the magnetic detector covered only part of the total solid angle and neutral particles were not detected, we needed to use a Monte Carlo simulation to

determine how jet-like and isotropic hadronic events would differ in the detector. Events were generated according to either Lorentz-invariant phase space or a jet model in which phase space was modified by a matrix element squared of the form

$$M^2 = e^{-\left(\sum_i p_{\perp i}^2\right)/2b^2} , \tag{5}$$

where $\vec{p}_{\perp i}$ is the momentum perpendicular to the jet axis for the i^{th} particle. The sum is over all produced particles. The jet axis angular distribution was of the form

$$\frac{d\sigma}{d\Omega} \propto 1 + \alpha \cos^2\theta , \tag{6}$$

where θ is the polar angle relative to the e^+ beam. In both models only charged and neutral pions were produced, although some checks were performed using models which included etas, kaons, and nucleons. The charged-pion and neutral-pion multiplicities were given by separate Poisson distributions. The simulation included the geometric acceptance, trigger efficiency, momentum resolution ($\sigma_p/p = .013p$ (GeV/c)), conversion probability for photons from π^o decay, and all other known characteristics of the detector. Radiation of the initial e^+ and e^- was included. At each energy $E_{c.m.}$ the total multiplicity and ratio of charged pions to neutral pions for both models were obtained by fitting to the observed charged particle mean momentum and mean multiplicity. The parameter b in the jet model was chosen by fitting to the observed mean $p_\perp$ with respect to the observed jet axis. We used $\alpha = 1$ for the jet axis angular distribution in agreement with the measurement which will be described.

We found evidence for jet structure in the agreement of the observed S distributions with the jet model predictions as opposed to the phase-space model predictions for $E_{c.m.} \geq 4.8$ GeV.[7,13] The data peak toward low S in disagreement with the phase-space model. At 3.0 GeV the data agree with either model; the predictions of the two models are the same. In addition, the jet model momentum and $p_\perp$ distributions are in much better agreement with the data than are the phase-space model distributions.[13]

We were able to measure the jet axis angular distribution directly for a subset of the data at $E_{c.m.} = 7.4$ GeV. For this data the e^+ and e^- beams were transversely polarized due to synchrotron radiation and absence of depolarizing resonances. The beam polarization was useful because it induced an azimuthal asymmetry through the following general angular distribution for production through a single virtual photon:[14]

$$\frac{d\sigma}{d\Omega} \propto 1 + \alpha \cos^2\theta + P^2\alpha \sin^2\theta \cos 2\phi , \tag{7}$$

where ϕ is the azimuthal angle with respect to the plane of the storage ring, P is the transverse polarization of each beam, and α is given by

$$\alpha = \frac{\sigma_T - \sigma_L}{\sigma_T + \sigma_L} \quad . \tag{8}$$

σ_T and σ_L are the transverse and longitudinal production cross sections, respectively. Since the detector had a small range of acceptance in $\cos^2\theta$ but full acceptance in ϕ, the polarization was necessary to determine α for the jet axis. P^2 was determined from the QED reaction (2). After correction for incorrect jet axis determination using the Monte Carlo simulation, we measured $\alpha = 0.97 \pm 0.14$ for the produced jet axis angular distribution.[7,13] In terms of σ_L and σ_T this value of α corresponds to $\sigma_L/\sigma_T = 0.02 \pm 0.07$. The jet axis angular distribution is consistent with that for a pair of spin-1/2 particles. With $\alpha = 1$ the jet model correctly predicts the inclusive hadron $\cos^2\theta$ dependence as a function of hadron momentum.[7,13]

The jet model Monte Carlo simulation has been found to give a good, although not perfect, representation of the multihadronic data. It reproduces the sphericity distributions for whole events and the single particle inclusive momentum and angular distributions. Its most important use beyond the observation of jet structure itself is in the calculation of various efficiency corrections for the measurements of the total cross section and single particle inclusive distributions.

V. INCLUSIVE DISTRIBUTIONS IN VARIABLES RELATIVE TO THE JET DIRECTION

The limiting of transverse momentum relative to an axis for e^+e^- hadron production is evidence for jet structure. If this jet structure is due to quark-parton jets, inclusive distributions in variables relative to the quark direction, which is expected to be the jet direction, may give us information about the fragmentation of quarks into hadrons. The inclusive hadronic cross section might be expected to be factorizable into a function of momentum parallel to the jet axis and a function of momentum perpendicular to that axis. In addition, these inclusive distributions can be compared with similar distributions from other processes, such as leptoproduction and hadron-hadron interactions.

In order to investigate such questions we have measured inclusive distributions in Feynman x, rapidity, and transverse momentum relative to the jet axis. A preliminary attempt to measure these distributions was reported previously,[13] but these measurements, although correct as stated, suffered from a bias introduced in order to obtain a good determination of the jet axis. The measurements presented here are better representations of the "true" inclusive distributions, and the biases which may be introduced by the method of determining them are studied.

For each hadronic event with three or more detected charged particles we construct an observed jet axis as described in Section IV. The components of each particle momentum parallel to ($p_{\parallel}$) and perpendicular to ($p_{\perp}$) the jet axis

are then calculated, as shown in Fig. 6.

We can then produce observed inclusive distributions in $p_{||}$, $p_{\perp}$, and rapidity. The problem then is to correct these distributions for geometric acceptance, trigger bias, data analysis cuts, and incorrect determination of the jet axis. Studies were made using the jet model Monte Carlo simulation described in Section IV in which we knew the true jet axis for every event. It was found that the observed distributions in $p_{||}$ for all events were similar enough to the produced distributions that they could be corrected to give the true distributions. The reason for this was that in cases where the true jet direction was very different from the observed jet axis the detected particles had relatively low momenta and were nearly isotropic. The rapidity and $p_{\perp}$ distributions, however, were more sensitive to the correct determination of the jet axis and could not be reasonably corrected for all events. The method used for these distributions will be described later.

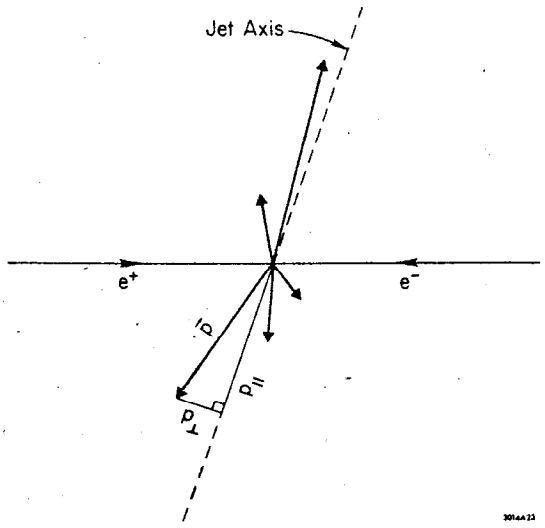

Figure 6. Illustration of a hadronic event from e^+e^- annihilation showing the jet axis and the components of the momentum $\vec{p}$ of a particle parallel to ($p_{||}$) and perpendicular to ($p_{\perp}$) the jet axis.

Since the inclusive quantity s $d\sigma/dx$, which was shown in Fig. 4, nearly scales, we are led to examine the inclusive distributions for s $d\sigma/dx_{||}$, where $x_{||}$, or Feynman x, is defined by

$$x_{||} = 2p_{||} / E_{c.m.} \quad . \tag{9}$$

In quark-parton models $x_{||}$ is the fraction of parton momentum carried by the hadron in the direction of the parton. The distributions s $d\sigma/dx_{||}$, corrected for acceptance, trigger bias, data analysis cuts, incorrect jet axis determination, and initial-state radiation are shown in Fig. 7 for the $E_{c.m.}$ values considered in Section III.

If we compare the distributions in s $d\sigma/dx_{||}$ with those in s $d\sigma/dx$, we see that as $E_{c.m.}$ increases the two distributions become more alike because $p_{\perp}$ is a decreasing fraction of p. At the lower energies the two distributions have quite different shapes. When e^+e^- inclusive momentum distributions are compared, for example, with leptoproduction, they should be compared in terms of the variable $x_{||}$. Except for the $E_{c.m.} = 3.0$ GeV data, the s $d\sigma/dx_{||}$ distributions scale for $0.1 < x_{||} < 0.8$ to within 10% which is at the level of our normalization and systematic uncertainties. For $E_{c.m.} \geq 4.8$ GeV scaling in s $d\sigma/dx_{||}$ appears to work better than scaling in s $d\sigma/dx$.

In order to measure the inclusive distributions in $p_\perp$ and rapidity we need to require that a fairly high momentum particle be detected in order to be able to find an observed jet axis which is close enough to the true jet direction that we can use the jet model Monte Carlo simulation to calculate corrections. However, requiring that a high momentum particle be detected biases the inclusive distributions. A method which can be used to remove the bias is the following:

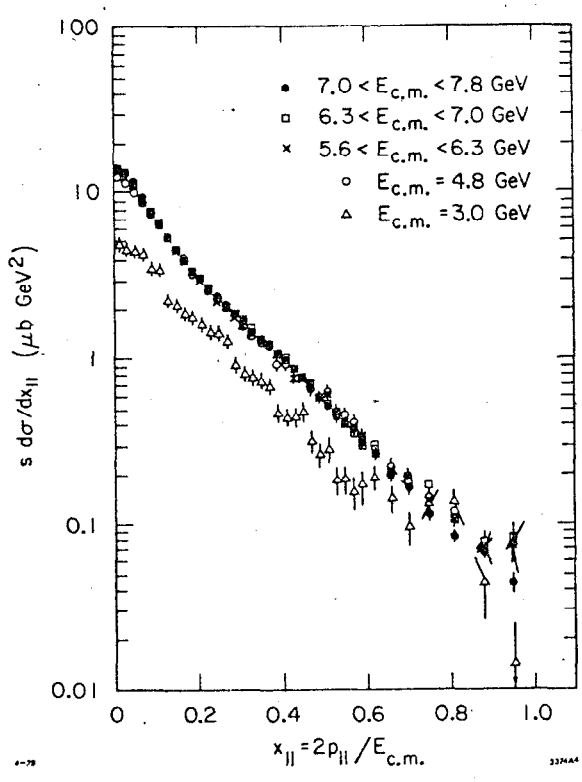

Fig. 7. Single particle inclusive $x_{||}$ distributions $s\, d\sigma/dx_{||}$ vs. $x_{||}$ for various $E_{c.m.}$. $x_{||} = 2p_{||}/E_{c.m.}$, where $p_{||}$ is the component of particle momentum parallel to the jet direction.

1. Find the observed jet axis in the usual way.
2. Divide the event into two jets with a plane through the interaction vertex and perpendicular to the jet axis.
3. If the highest-momentum particle on one side of the plane (x_{max}) has x greater than some minimum value, orient the jet axis to have a direction within 90° of this highest-momentum particle and measure the inclusive distributions in $x_{||}$, $p_\perp$, and rapidity for all the particles on the other side of the plane.
4. Repeat this procedure for the other side of the plane. This means that an event may be counted twice in the inclusive distributions, but no particle is counted more than once. The inclusive distributions are normalized to the total number of jets contributing.

Corrections are calculated by applying this procedure to both the produced and detected events in the jet model Monte Carlo simulation. For the produced events we know the true jet direction, so we can calculate corrections for finding the wrong jet axis in the detected events. The corrections, of course, are somewhat model dependent. We have some confidence in this correction procedure, however, because the jet model distributions agree rather well with the data.

As a test of the effectiveness of this method for removing biases due to requiring a high momentum particle, we apply it to the $x_{||}$ distributions which we have already measured for all events. We used the highest energy data sample, $7.0 < E_{c.m.} < 7.8$ GeV, because it has the best statistics (and also because it

should have the best-defined jet structure). In Fig. 8 are shown the distributions $(1/\sigma)d\sigma/dx_{||}$ versus $x_{||}$ for various cuts on x_{max} (which is at positive $x_{||}$ and is not plotted) for $7.0 < E_{c.m.} < 7.8$ GeV. σ is the cross section for jets with x_{max} within the specified range and the distributions $(1/\sigma)d\sigma/dx_{||}$ are thus distributions of particle density in $x_{||}$. The distributions are corrected for acceptance, trigger bias, data analysis cuts, incorrect jet axis determination, and initial-state radiation using the jet model Monte Carlo simulation and are therefore our best estimates of the true distributions. We see

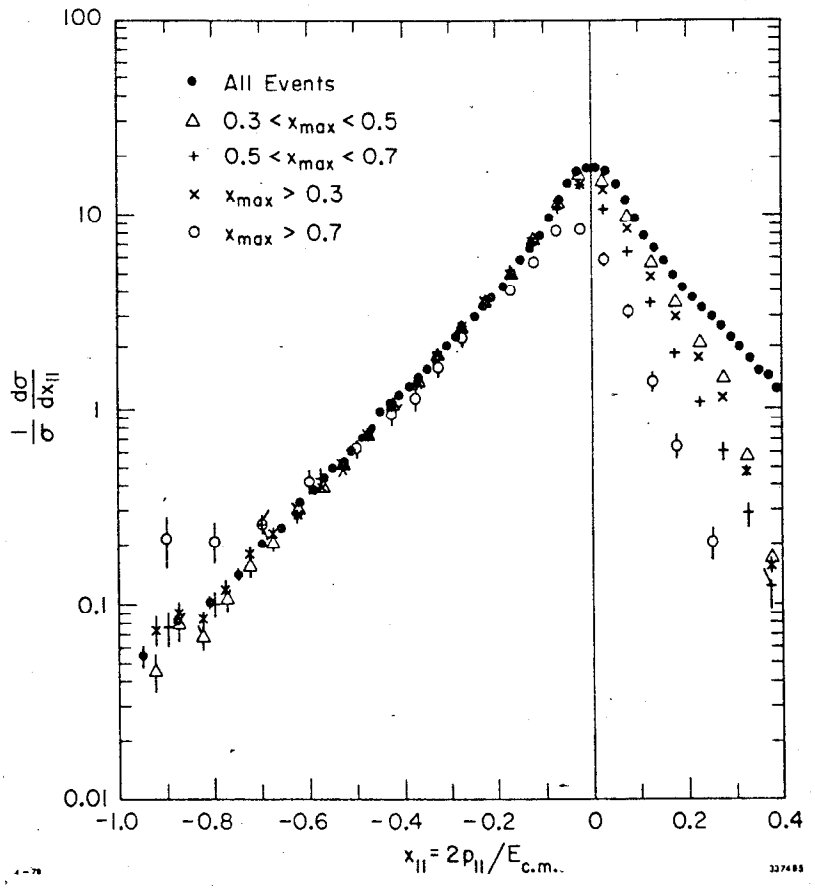

Fig. 8. Particle density distributions $(1/\sigma)d\sigma/dx_{||}$ vs. $x_{||}$ for various x_{max} cuts for $7.0 < E_{c.m.} < 7.8$ Gev. x_{max} is the highest-x particle on one side of the event and is not plotted. The jet direction is oriented so that x_{max} is at positive $x_{||}$. The distributions are normalized to the cross sections for jets with x_{max} within the specified range.

that these distributions are nearly independent of the x_{max} cut and agree with the distribution for all events for negative $x_{||}$. Only for $x_{max} > 0.7$ do we see a significant effect in the $x_{||}$ distribution on the opposite side: requiring a particle with $x_{max} > 0.7$ reduces the multiplicity for small $|x_{||}|$ and increases the multiplicity for large $|x_{||}|$. On the same side as the x_{max} particle we do see a correlation: the multiplicity decreases as x_{max} increases. We conclude that this method produces a relatively bias-free $x_{||}$ distribution for negative $x_{||}$; the $x_{||}$ distribution opposite a jet with $x_{max} > 0.3$ looks like the $x_{||}$ distribution for all events. We choose to use $x_{max} > 0.3$ for our analysis because the statistics are best. Of those observed jets with $x_{max} > 0.3$, only 4.7% have $x_{max} > 0.7$, so the difference in distributions for $x_{max} > 0.7$ has little effect. In fact, we have made a physical observation: we have shown that the $x_{||}$ distribution in one jet is independent of the x_{max} cut in the other jet. There is no particular reason why this has to be so. In Fig. 9 we show the $(1/\sigma)d\sigma/x_{||}$ distributions produced by

the jet model Monte Carlo calculation. The Monte Carlo shows a dependence of the negative $x_{||}$ distribution on the x_{max} cut used on the opposite side. For the Monte Carlo the multiplicity for small $|x_{||}|$ decreases and that for large $|x_{||}|$ increases as x_{max} increases. The $x_{||}$ distribution opposite a jet with $x_{max} > 0.3$ is significantly different from the distribution for all events.

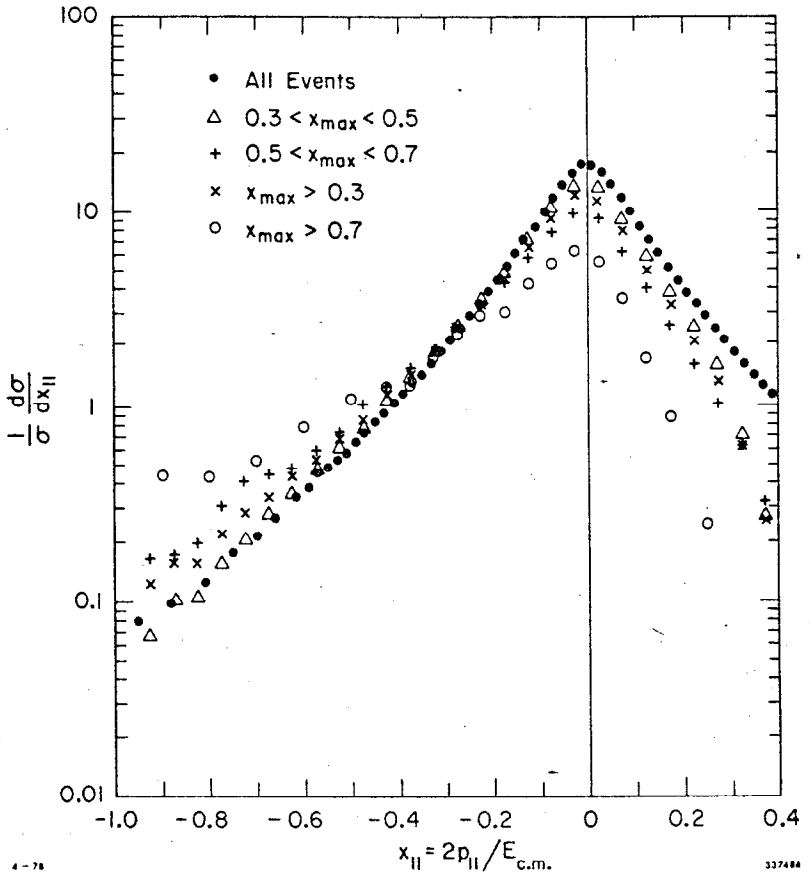

Fig. 9. Particle density distributions $(1/\sigma)d\sigma/dx_{||}$ vs. $x_{||}$ for various x_{max} cuts for jet model Monte Carlo at $E_{c.m.} = 7.276$ GeV.

The corrected $(1/\sigma)$ $d\sigma/dx_{||}$ distributions for $x_{max} > 0.3$ for various $E_{c.m.}$ values are shown in Fig. 10. $(1/\sigma)d\sigma/dx_{||}$ distributions for all events at the same energies are shown in Fig. 11. Here σ is the event cross section. The distributions in Fig. 10 for negative $x_{||}$ agree quite well with those in Fig. 11 for all $x_{||}$ considered to be positive if those in Fig. 11 are divided by two (because the distributions in Fig. 11 are for both jets). We see that the method works well for all energies; the $x_{||}$ distributions opposite a jet with $x_{max} > 0.3$ look like those for all events. To obtain $(1/\sigma)d\sigma/dx_{||}$ for all events from $(1/\sigma)d\sigma/dx_{||}$ for particles opposite a jet with $x_{max} > 0.3$, assume that the distribution for positive $x_{||}$ is the reflection of that for negative $x_{||}$ about $x_{||} = 0$. Then, since the distribution is symmetric about $x_{||} = 0$, it can be folded over at $x_{||} = 0$ so all particles are at positive $x_{||}$. One observation that can be made about the distributions $(1/\sigma)d\sigma/dx_{||}$ for various energies is that they scale rather well for all energies, including 3.0 GeV, for $x_{||} \geq 0.2$. That $(1/\sigma)d\sigma/dx_{||}$ scales for $E_{c.m.} \geq 4.8$ GeV is not surprising since s $d\sigma/dx_{||}$ scales and R is approximately constant. However, R at 3.0 GeV is a factor of two smaller than R at the higher energies. Evidently, normalizing the inclusive distributions in $x_{||}$ to the total cross section rather than the luminosity makes up for this difference.

Inclusive distributions in rapidity and $p_{\perp}$ relative to the jet direction can

then be measured using the method just described. The rapidity y is defined by

$$y = \frac{1}{2} \ln\left(\frac{E+p_{||}}{E-p_{||}}\right), \quad (10)$$

where E is the energy of the particle assuming a pion mass and $p_{||}$ is the component of particle momentum parallel to the jet axis. In Fig. 12 are shown the corrected particle density distributions $(1/\sigma)d\sigma/dy$ versus y for various x_{max} cuts for $7.0 < E_{c.m.} < 7.8$ GeV. As was the case for $(1/\sigma)d\sigma/dx_{||}$ for negative $x_{||}$, we see that the distributions for negative y are nearly independent of the x_{max} cut.

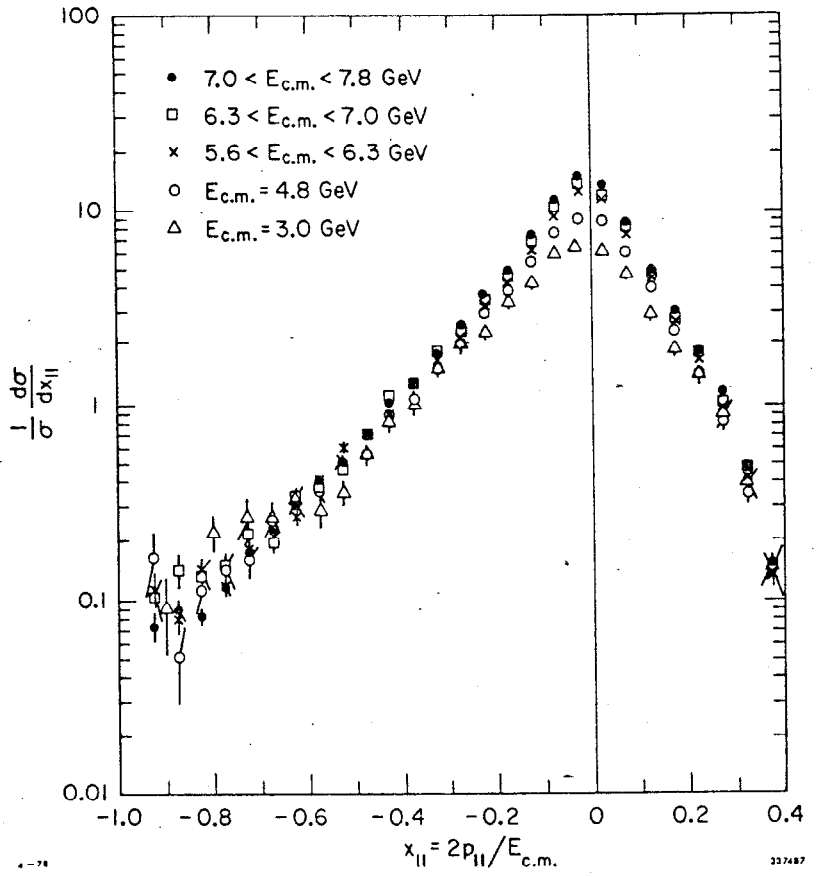

Fig. 10. Particle density distributions $(1/\sigma)d\sigma/dx_{||}$ vs. $x_{||}$ for $x_{max} > 0.3$ for various $E_{c.m.}$. x_{max} is at positive $x_{||}$ and is not plotted. The distributions are normalized to the cross sections for jets with $x_{max} > 0.3$.

For $x_{max} > 0.7$ there is a decrease in particle density for y between -1.5 and 0. For positive y, of course, we see a decrease in multiplicity as the x_{max} cut increases, as was shown previously for the $x_{||}$ distributions. We then used the cut $x_{max} > 0.3$ to produce corrected distributions in rapidity density at the other energies, as shown in Fig. 13. The distributions for negative y are our best estimates of the true rapidity distributions; those for positive y are distorted by the x_{max} cut. The real distributions of particles in rapidity relative to the jet direction would look like Fig. 13 with the distributions for positive y given by a reflection of those for negative y about y = 0. The distributions $(1/\sigma)d\sigma/dy$ increase in width as $E_{c.m.}$ increases. The distributions for the three highest energy ranges are quite similar in shape and appear to level off to a kind of plateau for y between -1.0 and 0. The value of $(1/\sigma)d\sigma/dy$ at the plateau is about 1.45 and is somewhat energy-dependent. A dip in $(1/\sigma)d\sigma/dy$ for y between -0.2 and 0 may be due to systematic errors in our data analysis. Because of tracking problems, we do not use particles with transverse momentum relative to the beam direction less than 150 MeV/c and must rely on the Monte Carlo simulation to

correct for this cut.

Distributions in $p_\perp$ relative to the jet direction are of some interest because they are the basis of the definition of jet structure. Jets occur because $p_\perp$ is limited as $E_{c.m.}$ increases. Figure 14 shows the corrected distributions $(1/\sigma)d\sigma/dp_\perp^2$ versus $p_\perp^2$ for particles opposite (negative $x_\parallel$) jets with various x_{max} cuts for $7.0<E_{c.m.}<7.8$ GeV. The distributions are independent of the x_{max} cut, except for $x_{max}>0.7$ which shows a decrease in particle density for $p_\perp^2<0.6(GeV/c)^2$. The corrected distributions $(1/\sigma)d\sigma/dp_\perp^2$ versus $p_\perp^2$ for the various $E_{c.m.}$ values measured for particles opposite jets with $x_{max}>0.3$ are presented in Fig. 15. The $p_\perp^2$ distributions are very similar in shape for $E_{c.m.}\geq 4.8$ GeV. The area under each curve increases as $E_{c.m.}$ increases because of the increasing multiplicity. For $E_{c.m.}=3.0$ GeV the $p_\perp^2$ distribution falls off slightly faster as $p_\perp^2$ increases and there are no particles with $p_\perp^2>0.6$ $(GeV/c)^2$. For events,

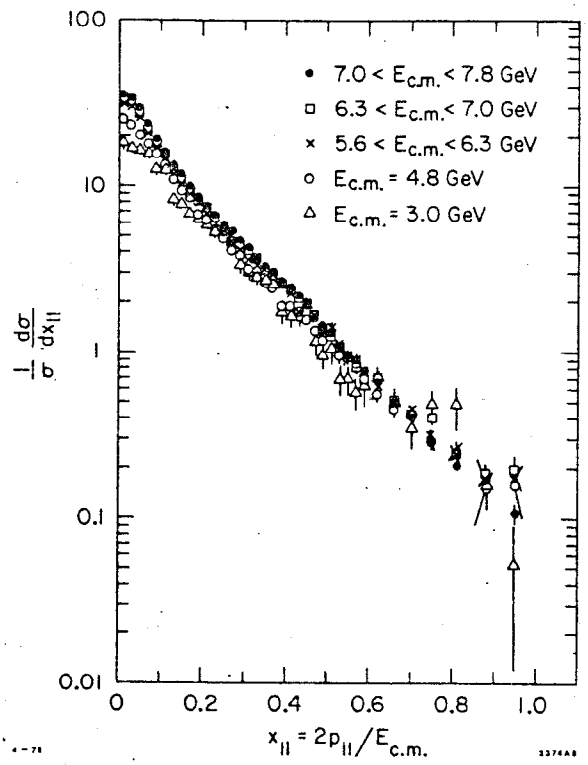

Fig. 11. Particle density distributions $(1/\sigma)d\sigma/dx_\parallel$ vs. $x_\parallel$ for all events for various $E_{c.m.}$. The distributions are normalized to the total cross sections for multihadronic events.

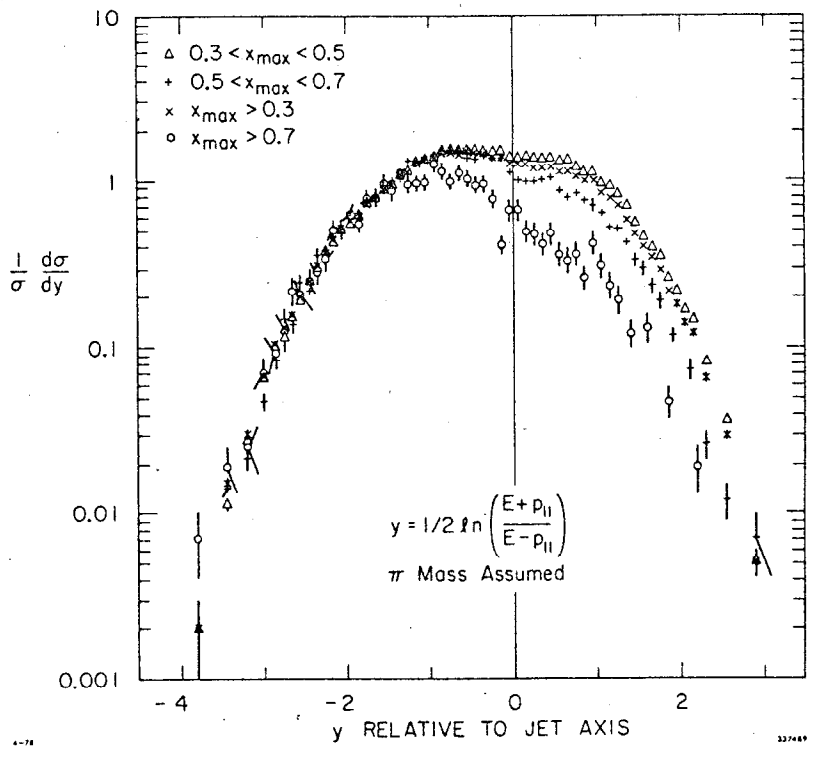

Fig. 12. Particle density distributions $(1/\sigma)d\sigma/dy$ vs. y for various x_{max} cuts for $7.0<E_{c.m.}<7.8$ GeV. x_{max} is the highest-x particle on one side of the event and is not plotted. The jet direction is oriented so that x_{max} is at positive y. The distributions are normalized to the cross sections for jets with x_{max} within the specified range.

be multiplied by two since they represent only one of the two jets.

The distributions shown in Fig. 15 have been corrected using the Monte Carlo jet model to calculate losses due to acceptance, trigger bias, and data analysis cuts and to calculate corrections due to finding the jet axis incorrectly. In order to show how these corrections might affect the $p_\perp^2$ distributions we present in Fig. 16 the uncorrected observed distributions $(1/N_{ev})dN/dp_\perp^2$ for particles opposite jets with $x_{max}>0.3$, where N_{ev} is the number of observed jets with $x_{max}>0.3$ and $dN/dp_\perp^2$ is the number of particles observed per $(GeV/c)^2$ in each $p_\perp^2$ bin. By comparing Figs. 15 and 16 one can see that the effect of the Monte Carlo corrections is to increase the particle density at high $p_\perp^2$ relative to that at low $p_\perp^2$. This is a reasonable efficiency correction because the detector acceptance makes it more difficult to detect both a jet and a particle at high $p_\perp$ to it. In any case, the Monte Carlo corrections do not change appreciably the similarity in shapes of the distributions for $E_{c.m.}\geq 4.8$ GeV nor do they change the observation that the slopes decrease as $p_\perp^2$ increases.

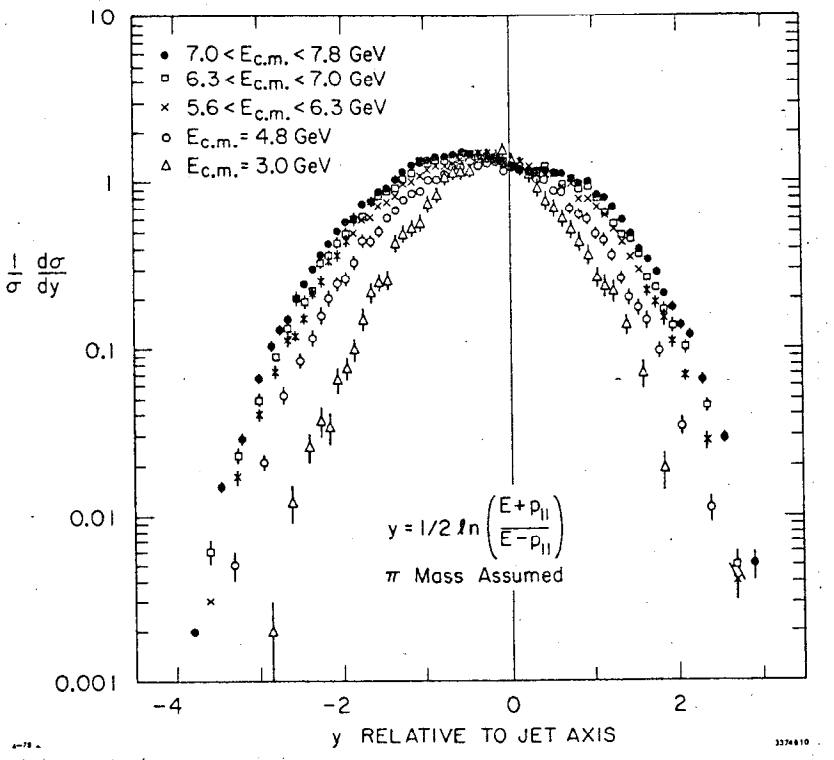

Fig. 13. Particle density distributions $(1/\sigma)d\sigma/dy$ vs. y for $x_{max}>0.3$ for various $E_{c.m.}$. y is the rapidity of the particle relative to the jet direction assuming a pion mass. x_{max} is at positive y and is not plotted. The distributions are normalized to the cross sections for jets with $x_{max}>0.3$.

Figure 17 shows the same distributions as in Fig. 15 plotted versus $p_\perp$ rather than $p_\perp^2$. These distributions are used to calculate the average transverse momentum relative to the jet direction $\langle p_\perp \rangle$ for each of the $E_{c.m.}$. Figure 18 shows $\langle p_\perp \rangle$ opposite jets with $x_{max}>0.3$ versus $E_{c.m.}$. The dependence of $\langle p_\perp \rangle$ on $E_{c.m.}$ is simple evidence for jet structure since $\langle p_\perp \rangle$ levels off as $E_{c.m.}$ increases. The value of $\langle p_\perp \rangle$ for $7.0<E_{c.m.}<7.8$ GeV is 364±2 MeV/c where the error is statistical only. To estimate the systematic error we calculated $\langle p_\perp \rangle$ for various x_{max} cuts for $7.0<E_{c.m.}<7.8$ GeV (see Fig. 14 for $p_\perp^2$ distributions for these x_{max} cuts). The range of $\langle p_\perp \rangle$ for different x_{max} cuts was within ±10 MeV/c of $\langle p_\perp \rangle$ for $x_{max}>0.3$,

Fig. 14. $(1/\sigma)d\sigma/dp_\perp^2$ vs. $p_\perp^2$ for particles opposite jets with various x_{max} cuts for $7.0<E_{c.m.}<7.8$ GeV. $p_\perp$ is the component of particle momentum perpendicular to the jet direction. The distributions are normalized to the cross sections for jets with x_{max} within the specified range.

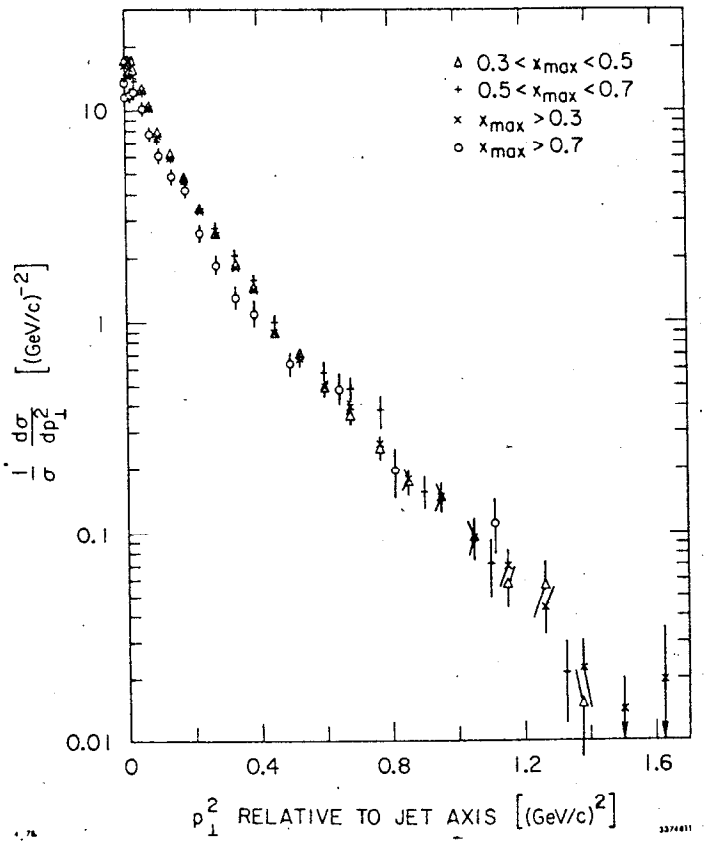

Fig. 15. $(1/\sigma)d\sigma/dp_\perp^2$ vs. $p_\perp^2$ for particles opposite (negative $x_\parallel$) jets with $x_{max}>0.3$ for various $E_{c.m.}$. $p_\perp$ is the component of particle momentum perpendicular to the jet direction. The distributions are normalized to the cross sections for jets with $x_{max}>0.3$. The solid lines represent the fits, discussed in the text, to the distributions for $E_{c.m.} = 3.0$ GeV and $7.0<E_{c.m.}<7.8$ GeV.

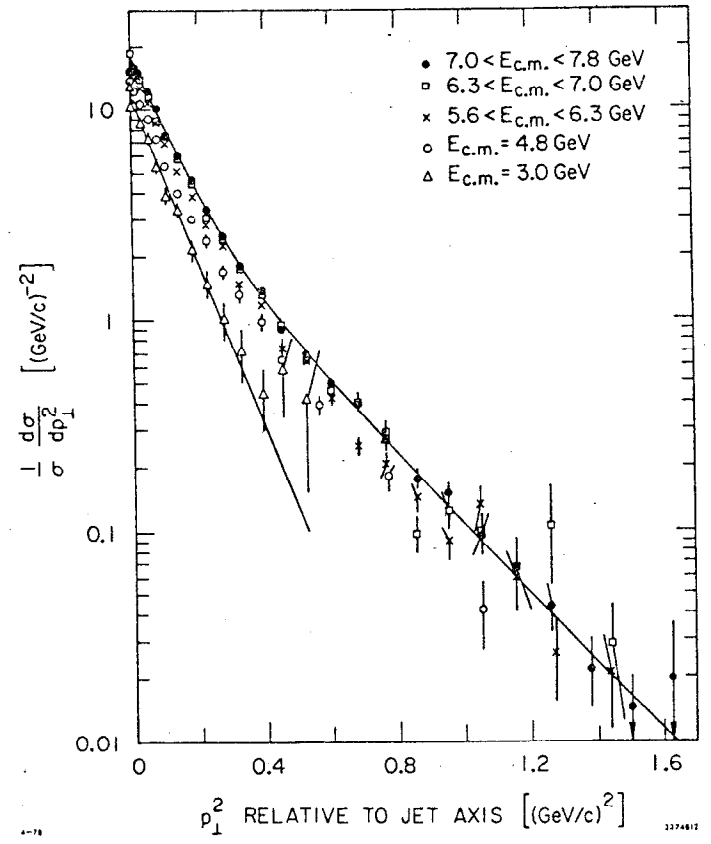

Fig. 16. Observed $(1/N_{ev})dN/dp_\perp^2$ for particles opposite jets with $x_{max}>0.3$ in events with 3 or more charged particles. N_{ev} is the number of observed jets with $x_{max}>0.3$ and $dN/dp_\perp^2$ is the number of particles observed per $(GeV/c)^2$ in each $p_\perp^2$ bin.

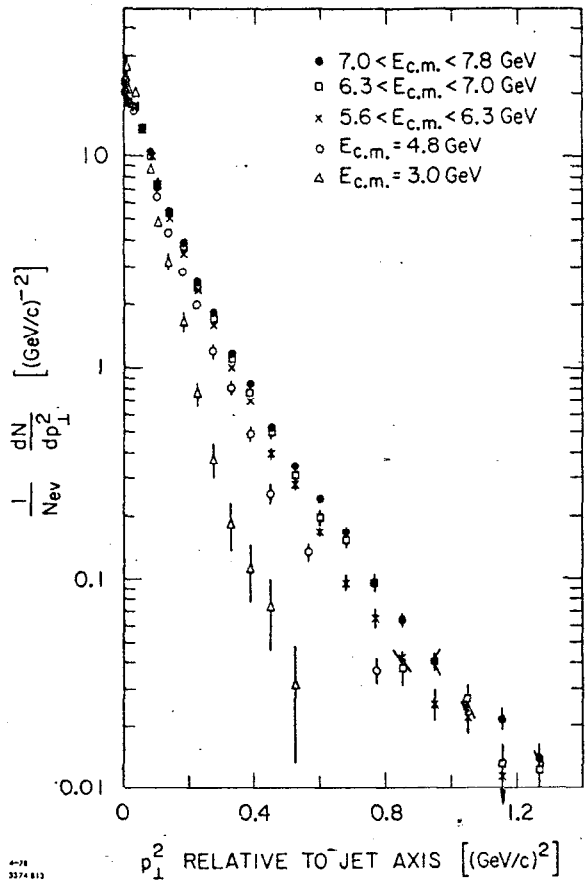

Fig. 17. $(1/\sigma)d\sigma/dp_\perp$ vs. $p_\perp$ for particles opposite jets with $x_{max}>0.3$ for various $E_{c.m.}$. $p_\perp$ is the component of particle momentum perpendicular to the jet direction. The distributions are normalized to the cross sections for jets with $x_{max}>0.3$.

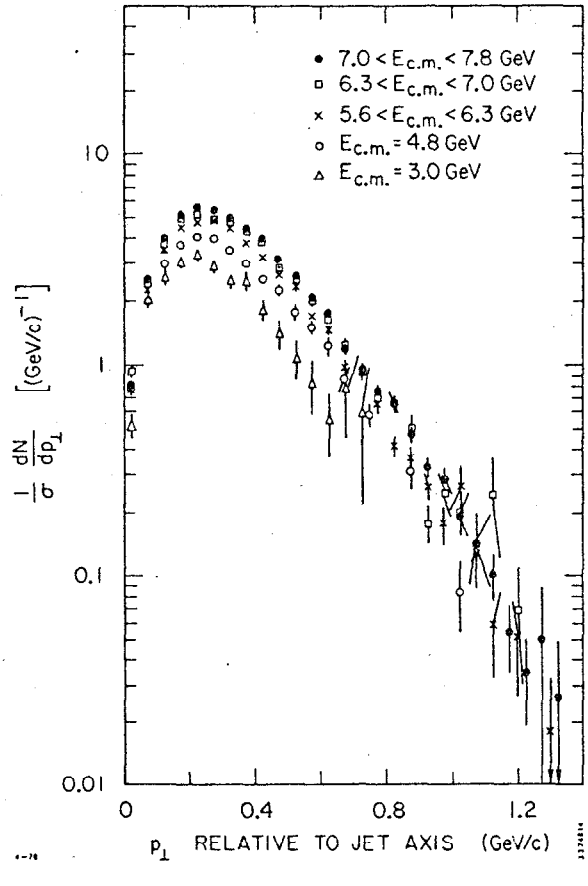

so we estimate the systematic error for $\langle p_\perp \rangle$ to be ±10 MeV/c.

The distributions $(1/\sigma)d\sigma/dp_\perp^2$ versus $p_\perp^2$, shown in Fig. 15, do not fit single exponentials in $p_\perp^2$, except for $E_{c.m.}$=3.0 GeV. The parameters for such attempted fits are listed in Table I. The χ^2/(degree of freedom) are very large for $E_{c.m.} \geq 4.8$ GeV. That a single exponential in $p_\perp^2$ is a poor fit for these energies is obvious from Fig. 15 since the slopes vary with $p_\perp^2$. For $E_{c.m.} \geq 4.8$ GeV the $p_\perp^2$ distributions fit reasonably well to a sum of two exponentials in $p_\perp^2$: $(1/\sigma)d\sigma/dp_\perp^2 = c_1 e^{-b_1 p_\perp^2} + c_2 e^{-b_2 p_\perp^2}$; the parameters for such fits are given in Table II. Only statistical errors were used to determine χ^2. The distributions given by the single exponential fit for $E_{c.m.}$=3.0 GeV and by the sum-of-two-exponentials fit for $7.0 < E_{c.m.} < 7.8$ GeV are represented by the solid lines in Fig. 15. The coefficients of $p_\perp^2$, b_1 and b_2, are plotted versus $E_{c.m.}$ in Figs. 19a and 19b. The larger coefficient b_1 is consistent with about 10 $(GeV/c)^{-2}$ for the three highest energy ranges; it is a little larger at $E_{c.m.}$ =4.8 GeV and a little smaller at $E_{c.m.}$ = 3.0 GeV. The smaller coefficient b_2 is consistent with about 4 $(GeV/c)^{-2}$ for all energies $E_{c.m.} \geq 4.8$ GeV. We have shown quantitatively that the shapes of the $p_\perp^2$ distributions are quite similar for $E_{c.m.} \geq 4.8$ GeV.

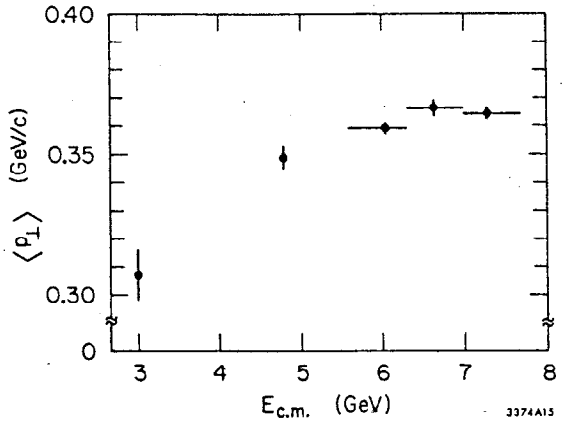

Fig. 18. Average transverse momentum relative to the jet direction $\langle p_\perp \rangle$ for particles opposite jets with $x_{max}>0.3$ vs. $E_{c.m.}$

In Fig. 20 we compare the $p_\perp^2$ distribution for $7.0 < E_{c.m.} < 7.8$ GeV with that for the jet model Monte Carlo. We see that for $p_\perp^2 > 0.6$ $(GeV/c)^2$ the Monte Carlo distribution is lower than the data. $\langle p_\perp \rangle$ for the Monte Carlo distribution is 343 MeV/c, about 20 MeV/c lower than for the data. We also note that the Monte

TABLE I

Fits to $\frac{1}{\sigma}\frac{d\sigma}{dp_\perp^2} = c\,e^{-bp_\perp^2}$ for particles opposite jets with $x_{max}>0.3$ for various $E_{c.m.}$ for $p_\perp^2 > 0.01$ $(GeV/c)^2$.

$E_{c.m.}$ (GeV)	c $[(GeV/c)^{-2}]$	b $[(GeV/c)^{-2}]$	χ^2	degrees of freedom
3.0	11.08±0.45	8.95±0.42	10.40	11
4.8	12.03±0.24	6.96±0.14	92.19	13
5.6-6.3	14.18±0.17	6.64±0.07	240.25	21
6.3-7.0	14.99±0.21	6.40±0.08	182.23	20
7.0-7.8	16.03±0.14	6.43±0.05	472.34	23

TABLE II

Fits to $\frac{1}{\sigma}\frac{d\sigma}{dp_\perp^2} = c_1 e^{-b_1 p_\perp^2} + c_2 e^{-b_2 p_\perp^2}$ for particles opposite jets with $x_{max}>0.3$ for various $E_{c.m.}$ for $p_\perp^2>0.01$ $(GeV/c)^2$.

$E_{c.m.}$ (GeV)	c_1 $[(GeV/c)^{-2}]$	b_1 $[(GeV/c)^{-2}]$	c_2 $[(GeV/c)^{-2}]$	b_2 $[(GeV/c)^{-2}]$	χ^2	degrees of freedom
3.0	11.08 ±0.45	8.95 ±0.42	--	--	10.40	11
4.8	9.37 ±0.86	13.18 ±1.56	4.93 ±0.98	4.43 ±0.36	4.86	11
5.6-6.3	12.15 ±0.69	10.41 ±0.68	4.13 ±0.80	3.93 ±0.27	23.75	19
6.3-7.0	11.53 ±1.01	11.07 ±1.08	5.87 ±1.17	4.25 ±0.30	36.70	18
7.0-7.8	13.97 ±0.49	10.23 ±0.44	4.62 ±0.56	3.77 ±0.17	29.86	21

Carlo distribution is not a single exponential in $p_\perp^2$. What is the reason for the excess of high $p_\perp$ particles? After testing several hypotheses, we finally found an answer. In Figs. 21a and 21b are shown the $K^\pm\pi^\mp$ invariant mass distributions for $7.0<E_{c.m.}<7.8$ GeV for both particles with $p_\perp<0.8$ GeV/c and for one or both particles with $p_\perp \geq 0.8$ GeV/c. For the first case we see no signal, but for the second case we see a peak near the D^0 mass of 1863 MeV/c^2.[5] (The only other way that has been found to isolate a D^0 signal in the high-energy data is to require the $K\pi$ momentum to be greater than 1.5 GeV/c.[15]) We therefore have conclusive evidence that some of the high $p_\perp$ particles are the result of D^0 production and decay into $K^-\pi^+$. Other D decays have been studied by Monte Carlo, but of these the decay of a heavy particle into two charged particles is the primary source of particles with $p_\perp>0.8$ GeV/c. In fact, it is possible to produce a quite adequate representation of the observed $p_\perp^2$ distribution by adding to the jet model Monte Carlo a contribution from $D^{0*}\bar{D}^{0*}\pi^+\pi^-$, where $D^{0*}\to D^0\gamma$ or $D^0\pi^0$ and D^0 decays only to $K^-\pi^+$, as shown in Fig. 22. One should note that all high $p_\perp$ particles do not necessarily come from charmed particle decays, and we cannot show that the second exponential in $p_\perp^2$ is completely due to charm. Some high $p_\perp$ particles can

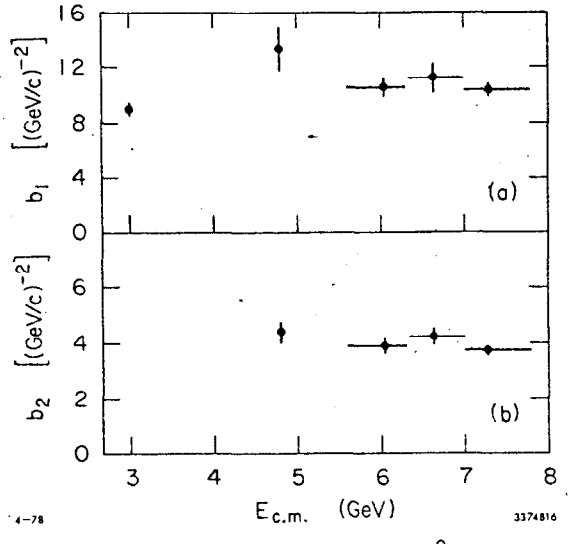

Fig. 19. Coefficients of $p_\perp^2$, (a) b_1 and (b) b_2, for fits of the form $(1/\sigma)d\sigma/dp_\perp^2 = c_1 e^{-b_1 p_\perp^2} + c_2 e^{-b_2 p_\perp^2}$ for particles opposite jets with $x_{max}>0.3$ vs. $E_{c.m.}$.

result from two-jet production, and the jet model $p_\perp^2$ distribution is not a single exponential in $p_\perp^2$.

We have measured the dependence of the $p_\perp$ distributions on $x_\parallel$, or Feynman x, for $7.0<E_{c.m.}<7.8$ GeV. Figure 23 shows the corrected distributions $(1/\sigma)d\sigma/dp_\perp^2$ versus $p_\perp^2$ for several $x_\parallel$ ranges for particles opposite jets with $x_{max}>0.3$. The distributions are normalized to the cross section for jets with $x_{max}>0.3$. From these distributions we see that particles with $x_\parallel$ between 0.1 and 0.3 are the major contributors to the high $p_\perp^2$ region. Particles with $x_\parallel$ less than 0.1 and between 0.3 and 0.5 contribute about equally to the high $p_\perp^2$ region. We were able to calculate $\langle p_\perp \rangle$ for the $x_\parallel$ ranges with $x_\parallel$ less than 0.5; the $p_\perp$ distributions for $x_\parallel$ greater than 0.5 are too poorly defined because of the limited statistics to allow a calculation of $\langle p_\perp \rangle$. In Fig. 24 we present $\langle p_\perp \rangle$ versus $x_\parallel$ for three $x_\parallel$ ranges. $\langle p_\perp \rangle$ increases with increasing $x_\parallel$ in a manner quite like the "seagull" effect seen in leptoproduction.[16]

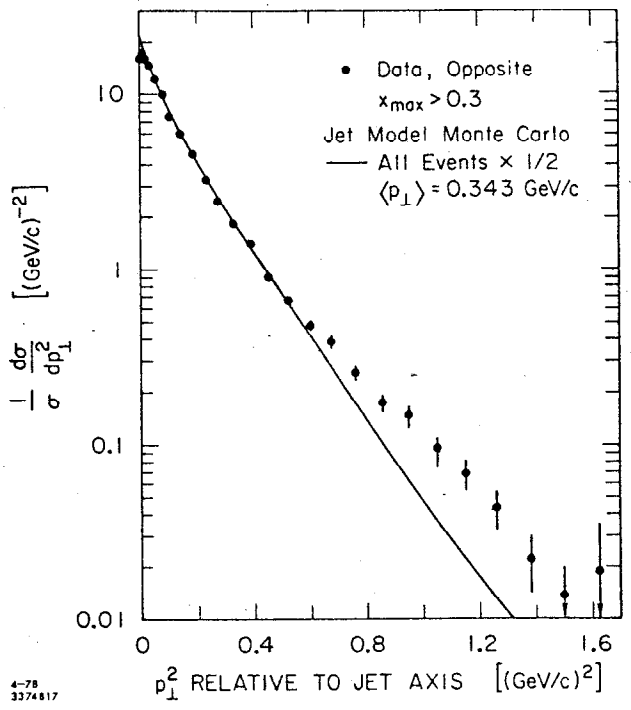

Fig. 20. Comparison of $(1/\sigma)d\sigma/dp_\perp^2$ vs. $p_\perp^2$ for particles opposite jets with $x_{max}>0.3$ for $7.0<E_{c.m.}<7.8$. GeV with the jet model Monte Carlo distribution for all events at $E_{c.m.}= 7.276$ GeV.

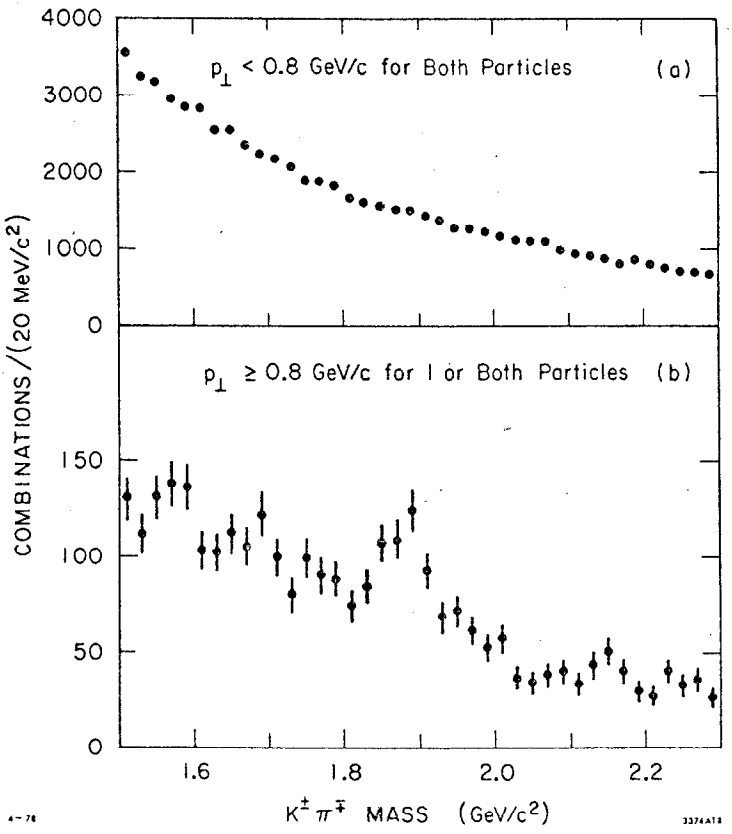

Fig. 21. $K^\pm\pi^\mp$ invariant mass distributions for $7.0<E_{c.m.}<7.8$ GeV for (a) both particles with $p_\perp<0.8$ GeV/c and (b) one or both particles with $p_\perp \geq 0.8$ GeV/c. $p_\perp$ is the component of particle momentum perpendicular to the observed jet axis. No time-of-flight information was used; each combination was plotted twice - once for each mass assignment.

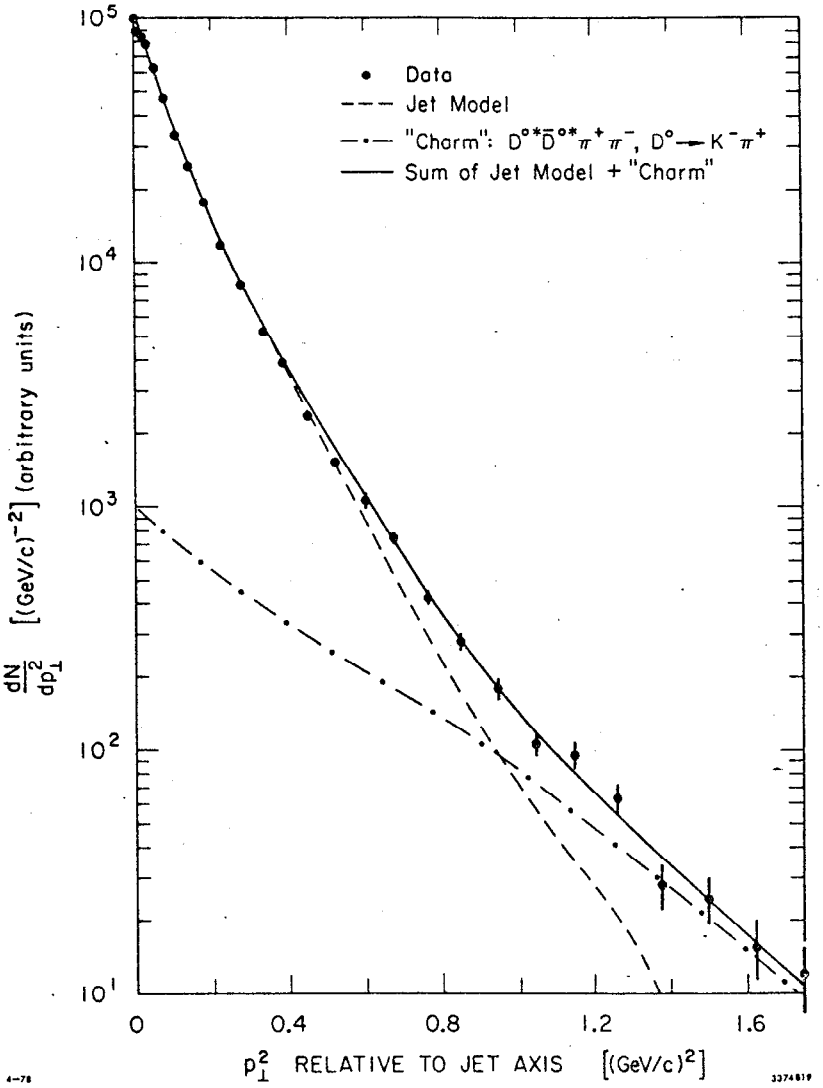

Fig. 22. Observed $p_\perp^2$ distribution for particles opposite jets with $x_{max}>0.3$ in events with 3 or more prongs for $7.0<E_{c.m.}<7.8$ GeV. $p_\perp$ is the component of particle momentum perpendicular to the observed jet axis. The data is compared with the sum of the Monte Carlo predictions of the jet model and a charmed meson production model. The Monte Carlo distribution is normalized to the total number of particles in the data. The relative normalization of the two models was chosen by requiring that the number of high $p_\perp^2$ particles agree with the data.

The $p_\perp^2$ distributions for $x_{||}<0.1$ and $0.1<x_{||}<0.3$ can be fitted to sums of two exponentials in $p_\perp^2$, and the distribution for $0.3<x_{||}<0.5$ requires only a single exponential. The parameters of the fits to $(1/\sigma)d\sigma/dp_\perp^2 = c_1e^{-b_1p_\perp^2} + c_2e^{-b_2p_\perp^2}$ are listed in Table III. The minimum $p_\perp^2$ used in the fits was varied somewhat to obtain reasonable fits. The fitted distributions are represented by the solid lines in Fig. 23. The values of the coefficients of $p_\perp^2$, b_1 and b_2, are plotted versus $x_{||}$ in Figs. 25a and 25b. Since the single coefficient for $0.3<x_{||}<0.5$ was

TABLE III

Fits to $\frac{1}{\sigma}\frac{d\sigma}{dp_\perp^2} = c_1 e^{-b_1 p_\perp^2} + c_2 e^{-b_2 p_\perp^2}$ for particles in various $x_{||}$ ranges opposite jets with $x_{max}>0.3$ for $7.0<E_{c.m.}<7.8$ GeV.

$x_{||}$ range	c_1 $[(GeV/c)^{-2}]$	b_1 $[(GeV/c)^{-2}]$	c_2 $[(GeV/c)^{-2}]$	b_2 $[(GeV/c)^{-2}]$	χ^2	degrees of freedom
<0.1 $p_\perp^2>0.09(GeV/c)^2$	8.98 ±0.47	10.37 ±0.72	0.96 ±0.33	3.79 ±0.41	19.17	15
0.1 - 0.3 $p_\perp^2>0.04(GeV/c)^2$	3.09 ±0.47	8.82 ±1.12	2.50 ±0.52	4.17 ±0.24	21.44	17
0.3 - 0.5 $p_\perp^2>0.16(GeV/c)^2$	1.24 ±0.09	3.88 ±0.21	--	--	15.69	11

in agreement with the smaller coefficient for the other two $x_{||}$ ranges, it was plotted in Fig. 25b. The larger coefficients for $x_{||}<0.1$ and $0.1<x_{||}<0.3$ are both consistent with 10 $(GeV/c)^{-2}$, the same value that was found for the $p_\perp^2$ distribution integrated over $x_{||}$. The smaller coefficients and the single coefficient for $0.3<x_{||}<0.5$ are consistent with 4 $(GeV/c)^{-2}$, again in agreement with the smaller coefficient for the $p_\perp^2$ distribution integrated over $x_{||}$. If we were to assume that the exponential with the smaller slope is due to charmed particle production, then we would be forced to conclude that all particles with $0.3<x_{||}<0.5$ are the result of charmed particle decay, which is unlikely. Unfortunately, we have been able to study only the decay $D^0\to K^-\pi^+$ which has a branching ratio of only (2.2±0.6)%.[5] We are otherwise unable to separate the charm production component in this analysis.

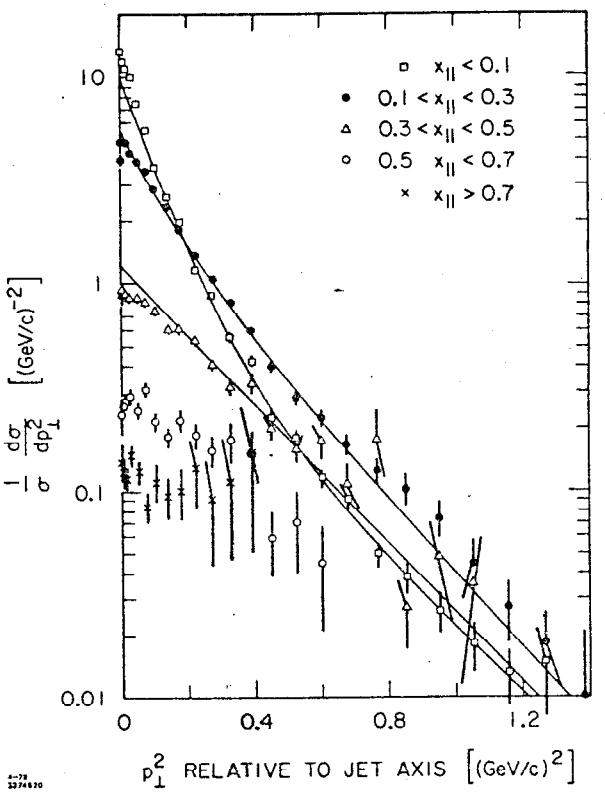

Fig. 23. $(1/\sigma)d\sigma/dp_\perp^2$ vs. $p_\perp^2$ for particles in various $x_{||}$ ranges opposite jets with $x_{max}>0.3$ for $7.0<E_{c.m.}<7.8$ GeV. The distributions are normalized to the cross section for jets with $x_{max}>0.3$.

We have looked for charge correlations between the leading particle in one jet and all other observed particles in events with three or more charged prongs. The data sample used was the highest energy range $7.0<E_{c.m.}<7.8$ GeV. We plotted $x_{||}$ distributions using the same method as was described in connection with Fig. 8, except that two distributions were produced - one for those particles with the same charge as x_{max} and another for those particles with the opposite charge to

the x_{max} particle. In Fig. 26 we present the observed ratio $\frac{\text{opposite charge}}{\text{same charge}}$ of these two distributions in $x_{||}$ for two different x_{max} cuts: $x_{max}>0.5$ and $x_{max}>0.7$. x_{max} is at positive $x_{||}$, and, of course, is not included. For this distribution we have used only events in which the total charge was 0 if an even number of particles was observed or ±1 if an odd number was observed. In general, since the detector did not have complete acceptance, one or more particles were not detected, so we do not expect to conserve charge. We also plotted the charged particle multiplicity distribution for each $x_{||}$ bin so that we could calculate the statistical expectation for the charge ratio. For example, for an event with 3 charged particles and total charge ±1 the probability that any 2 particles have opposite charge is 2/3 and the probability that any 2 particles have the same charge is 1/3, so the ratio of opposite charge to same charge is expected to be 2. The expected ratio decreases as the multiplicity increases. The statistical expectation versus $x_{||}$ is represented by the dashed line in Fig. 26. We see that for positive $x_{||}$ the ratio of opposite charge to same charge is much larger than the statistical expectation. This means that there are same-side correlations: particles in the same jet as the x_{max} particle tend to have the opposite charge to the x_{max} particle. Such an effect can be caused by neutral resonances and is expected for various other models. For negative $x_{||}$ there is no evidence for charge correlations. For $x_{max}>0.7$ the point at $x_{||}=-0.85$ is high compared with the statistical expectation, but the difference is not statistically significant. There were only

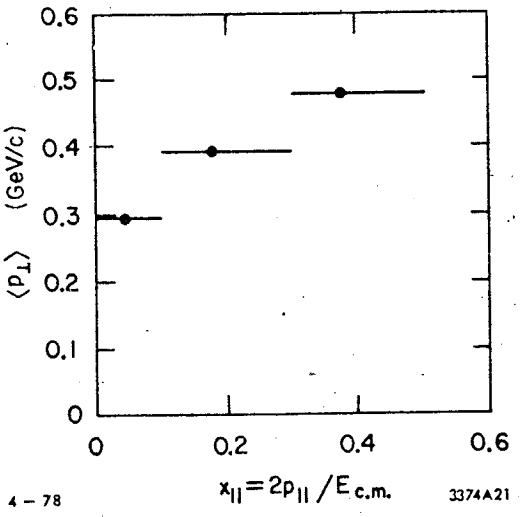

Fig. 24. Average transverse momentum relative to the jet direction $\langle p_\perp \rangle$ vs. $x_{||}$ for particles opposite jets with $x_{max}>0.3$ for $7.0<E_{c.m.}<7.8$ GeV.

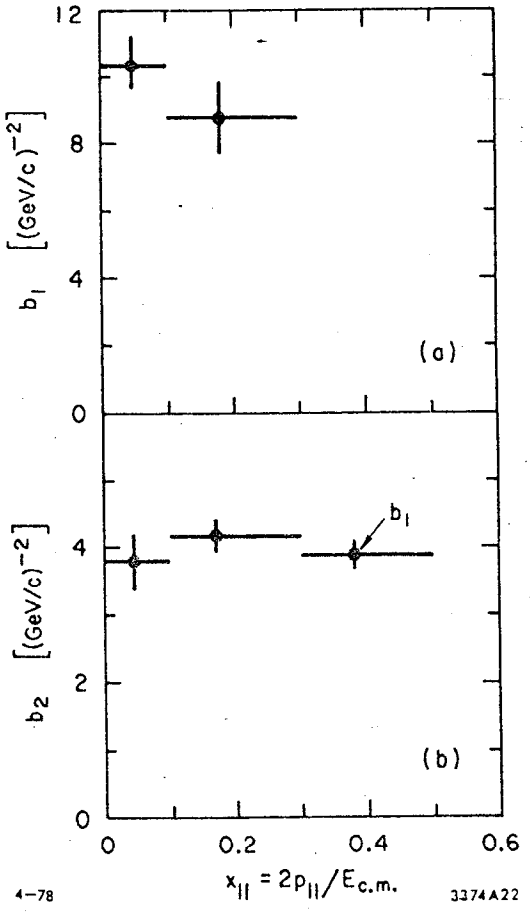

Fig. 25. Coefficients (a) b_1 and (b) b_2 for fits of the form $(1/\sigma)\,d\sigma/dp_\perp^2 = c_1 e^{-b_1 p_\perp^2} + c_2 e^{-b_2 p_\perp^2}$ vs. $x_{||}$ for particles opposite jets with $x_{max}>0.3$ for $7.0<E_{c.m.}<7.8$ GeV.

18 events contributing to this point. Of these 3 had the same charge as x_{max} and 15 had the opposite charge, whereas we would have expected 6 and 12. The probability of observing a charge ratio of 5 or more is about 10%. The statistical expectation is generally a little larger than the measured charge ratio for negative $x_{||}$. In principle, when calculating the statistical expectation for negative $x_{||}$ we should have taken into account the observed charge correlation at positive $x_{||}$. This would have had the effect of lowering the statistical expectation slightly for negative $x_{||}$. The effect would be small because the number of particles at positive $x_{||}$ is small for such large x_{max} cuts (see Fig. 8). Some quark-parton models predict a charge correlation between leading particles in opposite jets due to their production from a quark-antiquark pair. Particles at $x_{||}<-0.5$ are certainly the leading particles in the jet opposite the jet with x_{max}, yet we see no such effect. It may be that to see these leading-particle charge correlations, both particles must have x very near 1; unfortunately, the statistics of our data sample are not sufficient for such a measurement.

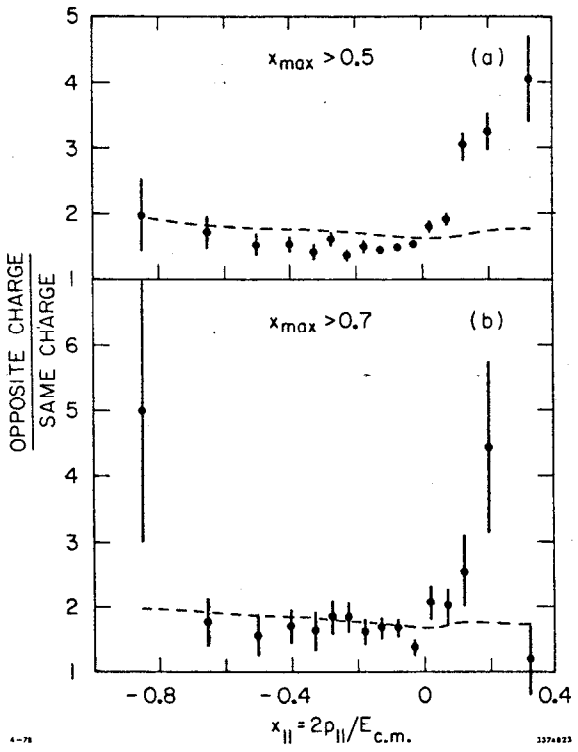

Fig. 26. Observed ratio of the number of particles with opposite charge to the x_{max} particle to the number of particles with the same charge as x_{max} for (a) $x_{max}>0.5$ and (b) $x_{max}>0.7$ vs. $x_{||}$ for $7.0<E_{c.m.}<7.8$ GeV. x_{max} is at positive $x_{||}$. The statistical expectations, calculated from the charged particle multiplicity distributions for each $x_{||}$ bin, are represented by the dashed lines.

VI. CONCLUSIONS

Studies of hadron production by e^+e^- annihilation have yielded very exciting results. The data discussed here were taken by the SLAC/LBL magnetic detector collaboration at SPEAR at center-of-mass energies between 2.6 and 7.8 GeV away from the resonance regions. The major results presented in this talk may be summarized as follows:

1. R, the ratio of the total hadronic cross section to the muon pair production cross section, shows the following behavior, apart from the ψ, ψ', and ψ'' peaks: below 3.5 GeV, R is approximately constant at a value of about 2.6; between 3.5 and 4.5 GeV, R shows a complex structure associated with charm production; above 4.8 GeV, R is again approximately constant

at a value of about 5.3 without subtracting heavy lepton production.

2. The single particle inclusive distributions s $d\sigma/dx$ roughly scale for $x \geq 0.3$ for the entire $E_{c.m.}$ range 3.0 to 7.8 GeV.
3. There is strong evidence for jet structure in hadronic events for $E_{c.m.} \geq 4.8$ GeV. At 7.4 GeV the jet axis angular distribution was measured to be proportional to $1 + (0.97 \pm 0.14) \cos^2\theta$, consistent with that for a pair of spin-1/2 particles. A jet model Monte Carlo simulation is able to reproduce the sphericity distributions and the single particle inclusive momentum and angular distributions for events with three or more charged particles.
4. Inclusive distributions in s $d\sigma/dx_{\parallel}$, where $x_{\parallel}$ (Feynman x) $= 2p_{\parallel}/E_{c.m.}$ and $p_{\parallel}$ is the component of particle momentum parallel to the jet direction, scale to within 10% for $0.1 < x_{\parallel} < 0.8$ for $E_{c.m.} \geq 4.8$ GeV. Inclusive distributions in $(1/\sigma)d\sigma/dx_{\parallel}$, where σ is the total hadronic cross section, scale rather well for $x_{\parallel} \geq 0.2$ for all energies.
5. The $x_{\parallel}$ distribution for one jet is nearly independent of the magnitude of the momentum of the leading particle in the other jet.
6. Distributions in rapidity with respect to the jet direction have been measured and show the development of a plateau for the three highest energy regions measured, from 5.6 to 7.8 GeV.
7. Distributions in $p_{\perp}^2$ relative to the jet direction have been measured. The average $p_{\perp}$ has been measured as a function of $E_{c.m.}$ and levels off at a constant value for the three highest energy regions measured, giving direct evidence for jet structure. The distributions in $p_{\perp}^2$ can be fitted to the sum of two exponentials in $p_{\perp}^2$. A contribution from charmed meson production needs to be added to the jet model in order to account for all of the high $p_{\perp}$ particles observed.
8. Distributions in $p_{\perp}^2$ as a function of $x_{\parallel}$ have been measured for $7.0 < E_{c.m.} < 7.8$ GeV. The average $p_{\perp}$ increases with increasing $x_{\parallel}$ for $x_{\parallel} \leq 0.5$.
9. Evidence for same-side charge correlations has been found: particles in the same jet as a large-x leading particle tend to have charge opposite to that of the leading particle. There is no evidence for opposite-side charge correlations.

The data seem to be in general agreement with the predictions of quark-parton constituent models. The production of charmed particles complicates the picture somewhat. It should be quite interesting to see what happens at the next higher-energy storage rings PEP and PETRA.

REFERENCES

1. See Gary J. Feldman and Martin L. Perl, Phys. Reports 33C, 285 (1977) and references therein.
2. See G.J. Feldman in Proceedings of Summer Institute on Particle Physics, SLAC-198 (Stanford Linear Accelerator Center, Stanford University, Stanford, California, 1976), p. 81, and references therein; W. Tanenbaum et al., SLAC-PUB-1987, to be published in Phys. Rev.
3. M.L. Perl et al., Phys. Lett. 70B, 487 (1977) and references therein.
4. See G.J. Feldman in Proceedings of Summer Institute on Particle Physics, SLAC-204 (Stanford Linear Accelerator Center, Stanford University, Stanford, California, 1977), p. 241, and references therein.
5. I. Peruzzi et al., Phys. Rev. Lett. 39, 1301 (1977).
6. S.D. Drell, D.J. Levy, and T.M. Yan, Phys. Rev. 187, 2159 (1969), and Phys. Rev. D 1, 1617 (1970); N. Cabibbo, G. Parisi, and M. Testa, Lett. Nuovo Cimento 4, 35 (1970); J.D. Bjorken and S.J. Brodsky, Phys. Rev. D 1, 1416 (1970); R.P. Feynman, Photon-Hadron Interactions (W.A. Benjamin, Inc., 1972), p. 166.
7. G. Hanson et al., Phys. Rev. Lett. 35, 1609 (1975).
8. Members of the SLAC/LBL Mark I magnetic detector collaboration were: G.S. Abrams, M.S. Alam, J.-E. Augustin, A.M. Boyarski, M. Breidenbach, D. Briggs, F. Bulos, W.C. Carithers, W. Chinowsky, J.T. Dakin, R.G. DeVoe, J.M. Dorfan, G.J. Feldman, G.E. Fischer, C.E. Friedberg, D. Fryberger, G. Goldhaber, G. Hanson, R.J. Hollebeek, J.A. Jaros, B. Jean-Marie, D.L. Hartill, A.D. Johnson, J.A. Kadyk, R.R. Larsen, A.M. Litke, D. Lüke, B.A. Lulu, V. Lüth, H.L. Lynch, D. Lyon, R.J. Madaras, C.C. Morehouse, H.K. Nguyen, J.M. Paterson, M.L. Perl, I. Peruzzi, M. Piccolo, F.M. Pierre, T.P. Pun, P. Rapidis, B. Richter, B. Sadoulet, R.H. Schindler, R.F. Schwitters, J. Siegrist, W. Tanenbaum, G.H. Trilling, F. Vannucci, J.S. Whitaker, F.C. Winkelmann, J.E. Wiss, and J.E. Zipse.
9. R.F. Schwitters in Proceedings of the International Symposium on Lepton and Photon Interactions at High Energies (Stanford University, Stanford, California, 1975), p. 5.
10. G. Grindhammer, talk presented at this conference.
11. J. Bürger, talk presented at this conference.
12. G. Wolf, talk presented at this conference.
13. Gail G. Hanson, Proceedings of the VIIth International Colloquium on Multiparticle Reactions (Tutzing, Germany, 1976), p. 313, and Proceedings of the XVIIIth International Conference on High Energy Physics (Tbilisi, U.S.S.R., 1976), p. B1.
14. Yung Su Tsai, Phys. Rev, D 12, 3533 (1975).

15. G.J. Feldman et al., Phys. Rev. Lett. 38, 1313 (1977).
16. See, for example, W.A. Loomis, et al., "Hadron Production in Muon-Proton and Muon-Deuteron Collisions," Harvard University preprint, submitted to Phys. Rev.